remote sensing

MDPI

Article

Analysis of Meteorological Drivers of Taihu Lake Algal Blooms over the Past Two Decades and Development of a VOCs Emission Inventory for Algal Bloom

Zihang Liao [1], Shun Lv [2], Chenwu Zhang [3], Yong Zha [1], Suyang Wang [4] and Min Shao [2,*]

[1] School of Geographic Sciences, Nanjing Normal University, Nanjing 210046, China; 221302175@njnu.edu.cn (Z.L.); yzha@njnu.edu.cn (Y.Z.)
[2] School of Environment, Nanjing Normal University, Nanjing 210046, China; 222502017@njnu.edu.cn
[3] School of the Environment, Nanjing University, Nanjing 210046, China; 522022250131@smail.nju.edu.cn
[4] Shanghai Rural Commercial Bank, Shanghai 200002, China; wangsy2@shrcb.com
* Correspondence: mshao@masonlive.gmu.edu

Abstract: Cyanobacterial blooms represent a common environmental issue in aquatic systems, and these blooms bring forth numerous hazards, with the generation of volatile organic compounds (VOCs) being one of them. Global climate change has led to alterations in various climatic factors affecting algal growth, indirectly impacting the quantity of VOCs released by algae. With advancements in remote sensing technology, exploration of the spatiotemporal distributions of algae in large water bodies has become feasible. This study focuses on Taihu Lake, characterized by frequent occurrences of cyanobacterial blooms. Utilizing MODIS satellite imagery from 2001 to 2020, we analyzed the spatiotemporal characteristics of cyanobacterial blooms in Taihu Lake and its subregions. Employing the LightGBM machine learning model and the (SHapley Additive exPlanations) SHAP values, we quantitatively analyzed the major meteorological drivers influencing cyanobacterial blooms in each region. VOC-related source spectra and emission intensities from cyanobacteria in Taihu Lake are collected based on the literature review and are used to compile the first inventory of VOC emissions from blue-green algae blooms in Taihu Lake. The results indicate that since the 21st century, the situation of cyanobacterial blooms in Taihu Lake has continued to deteriorate with increasing variability. The relative impact of meteorological factors varies across different regions, but temperature consistently shows the highest sensitivity in all areas. The VOCs released from the algal blooms increase with the proliferation of the blooms, posing a continuous threat to the atmospheric environment of the surrounding cities. This study aims to provide a scientific basis for further improvement of air quality in urban areas adjacent to large lakes.

Keywords: cyanobacteria; VOCs; MODIS; climate change; explainable machine learning

Citation: Liao, Z.; Lv, S.; Zhang, C.; Zha, Y.; Wang, S.; Shao, M. Analysis of Meteorological Drivers of Taihu Lake Algal Blooms over the Past Two Decades and Development of a VOCs Emission Inventory for Algal Bloom. *Remote Sens.* **2024**, *16*, 1680. https://doi.org/10.3390/rs16101680

Academic Editor: SeungHyun Son

Received: 14 April 2024
Revised: 3 May 2024
Accepted: 4 May 2024
Published: 9 May 2024

1. Introduction

Since the 1980s, the frequency and severity of cyanobacterial blooms in Taihu Lake have exhibited a discernible upward trend [1–3]. On multiple occasions, the repercussions of algal-bloom incidents have detrimentally impacted the lives of millions, significantly affecting critical aspects such as drinking water supply, tourism, and aquaculture in the adjacent urban centers [4]. Furthermore, at various life stages, cyanobacteria release (volatile organic compounds) VOCs [5], influencing both lake ecosystems and the atmosphere, particularly in the formation of tropospheric ozone and secondary organic aerosols (SOA) during algal blooms [6–14]. A profound understanding of how climate change influences the growth of algal blooms, the quantity of VOCs produced by these blooms, and the impact of VOCs on surrounding urban areas is crucial for further improvement of the environmental quality of Taihu Lake.

The growth of cyanobacterial blooms is influenced by various factors, categorized as external environmental factors and internal physiological and ecological characteristics. Internal physiological and ecological characteristics include unique cell structures that confer traits such as nitrogen fixation, CO_2 concentration mechanisms, buoyancy generation, and toxin production, providing cyanobacteria with a competitive advantage in phytoplankton competition [15–19]. External influencing factors are the primary drivers for the occurrence of cyanobacterial blooms. These factors include nutrients (nitrogen, phosphorus, nitrogen-phosphorus ratio, etc.) [20,21], physical variables of water bodies (temperature, transparency, etc.), hydrodynamic conditions (flow rate, hydraulic retention time, etc.) [22], biological variables (phytoplankton, filter-feeding fish, etc.), and meteorological factors (temperature, precipitation, wind speed, radiation duration, etc.).

Prior to the increased attention to global warming, nutrients were considered absolute controllers. However, with the drastic changes in global climate, meteorological factors such as temperature, precipitation, solar radiation, wind, etc., have exhibited significant variations [23,24]. These changes subsequently affect the hydrodynamics and biogeochemical processes of nutrients in lakes, increasing the frequency and intensity of cyanobacterial-bloom occurrences and posing a serious threat to lake ecosystem security and human health [25,26]. In the context of global climate change, algal blooms, exacerbated by meteorological conditions, pose a significant challenge.

The impact mechanism of meteorological conditions on cyanobacteria has been extensively studied, as evidenced by numerous research endeavors. For instance, temperature is a key factor influencing cyanobacterial growth, affecting various physicochemical processes in water [27–29]. Temperature influences various chemical and physical processes in the water, such as the dissolution, dissociation, or decomposition rates of substances like minerals and organic matter. These processes indirectly impact the photosynthesis of algae in aquatic environments. More importantly, temperature affects the reaction rates of photosynthetic enzymes, the rates of synthetic metabolism, and respiratory intensity within cyanobacteria, altering the overall photosynthetic yield and the net production process of algae. For rainfall impacts, Bouvy et al. [30] suggest that nutrients can be transferred into water bodies by rainfall, and at the same time, rainfall can increase water volume, dilute pollutants, lower water and air temperatures, and lead to a rise in lake levels, thereby altering the concentration of nutrients in the water. The importance of rainfall in affecting bloom occurrence is also reported by Reichwaldt et al. [31] and Wood et al. [32]. Solar radiation serves as the driving force for the photosynthetic process in algae. The photosynthetic rate of algae increases with increasing light intensity until it reaches the compensation point, where the rate of photosynthesis equals the rate of respiration. As light intensity continues to increase, the photosynthetic rate will also continue to rise until it reaches the light saturation point, at which the photosynthetic rate reaches its maximum value and remains steady. [31,32]. Wind is a crucial factor influencing hydrodynamics in aquatic environments. Studies indicate that when wind acts on the water surface, it induces turbulence, significantly impacting both the vertical and horizontal distribution of cyanobacteria. Excessive wind speed may submerge cyanobacteria underwater, preventing the formation of blooms. Conversely, low wind speeds result in a relatively smooth water surface with no wave action, causing cyanobacteria to float on the water, drift downwind, accumulate along windward shores, and form blooms [31,33,34].

Remote sensing, with its advantages of high spatial and temporal resolutions and low-cost detection, has been extensively used for land vegetation studies and cyanobacteria distribution monitoring [35–41]. Recently, decision trees, machine learning, and other methods were explored to enhance the accuracy of algal-bloom inference. It can be asserted that the satellite-based inference of extensive algal blooms has evolved into a relatively mature technology. The endeavor is noted in attempting to characterize regional VOC conditions through the inverse estimation of atmospheric column concentrations of VOCs [42–45]. Yet, the integration of remote sensing with cyanobacteria-released VOCs research is scarce.

This study investigates the impact of climate change on cyanobacterial blooms in Taihu Lake, one of China's major freshwater lakes located in eastern China. We performed a rigorous quantitative analysis using the LightGBM machine learning model and the SHAP (SHapley Additive exPlanations) method to identify and assess the primary climatic drivers influencing these blooms in each region of Taihu Lake. Additionally, we compiled an inventory of VOC emissions from cyanobacterial blooms based on source spectra and emission intensities. The study also provides a preliminary exploration of changes in VOC emissions from algal blooms in the context of climate change, offering reference data for investigating the impact of bloom-released VOCs on surrounding areas. Section 2 presents data and methods. Section 3 details the spatiotemporal characteristics of cyanobacterial blooms, VOC-emission patterns, and meteorological conditions observed in Taihu Lake through satellite data. Section 4 discusses the impact of meteorological factors on cyanobacterial blooms and the implications of the algal-bloom VOC inventory. A conclusion is given in Section 5.

2. Data and Methods

2.1. Study Area

Taihu Lake (30.56°–31.87°N, 119.54°–120.85°E, right panel of Figure 1) stands as the third-largest freshwater lake in China, encompassing an area of approximately 2338 square kilometers. By the year 2022, the lake's volumetric capacity reached 51.6 billion cubic meters, featuring a maximum depth of 4.8 m and an average depth of 1.9 m. Nestled within the economically advanced Yangtze River Delta (YRD) region (left panel of Figure 1), the Taihu Lake Basin [46,47], constitutes 4.8% of China's total population and contributes 9.8% to the nation's gross domestic product.

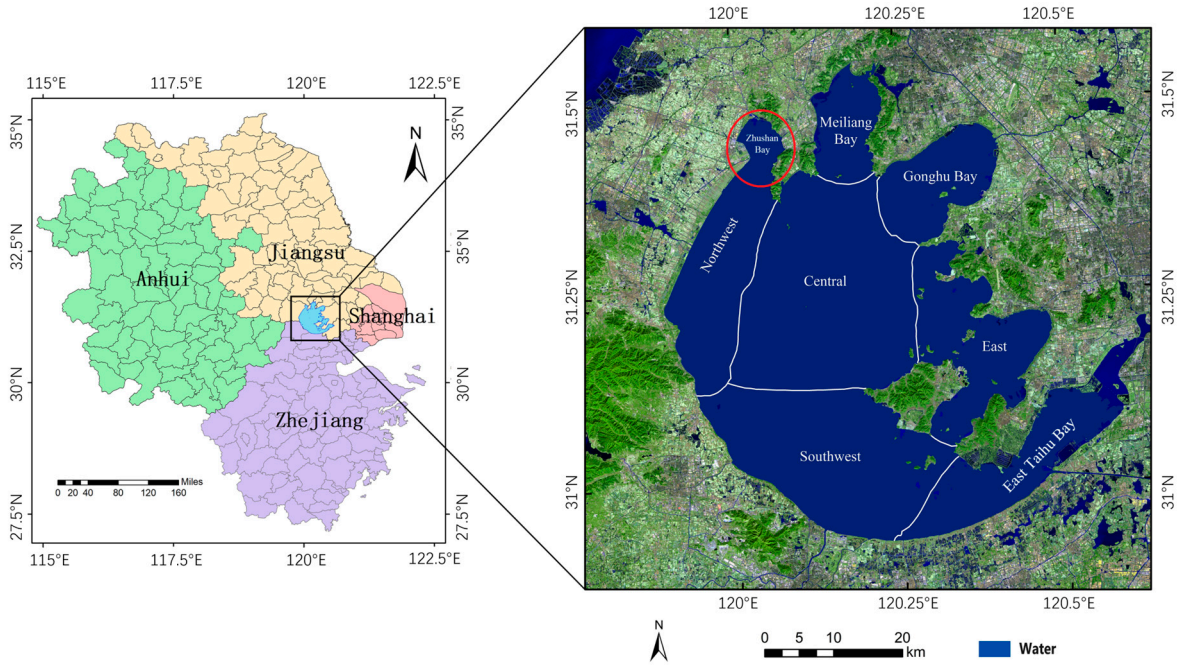

Figure 1. The location of Taihu Lake in the Yangtze River Delta region (**left panel**) and different regions of Taihu Lake (**right panel**) (red circle represents Zhushan Bay).

As shown in the right panel of Figure 1, Taihu Lake is further divided into 7 regions based on the lake's nutrient status, vegetation distribution, and hydraulic connectivity [47]. The name and description of each region are summarized in Table 1. This study predominantly focuses on the Northwest, Meiliang Bay, Gonghu Bay, Central, and Southwest regions of Taihu Lake. The selection of these regions is motivated by their recurrent exposure to the impacts of cyanobacterial blooms.

Table 1. Overview of Taihu Lake subdivisions.

Region	Description
Northwest	The primary inflow region, including Zhushan Bay (the very north part), receives ~80% of the total inflow, as well as most of the pollution.
Meiliang Bay	The region experiences frequent pollution, with the west affected by industrial and agricultural pollutants, and the north impacted by urban pollution.
Gonghu Bay	The key water source for two major cities, receiving river discharges for urban consumption
Central	Far offshore with the deepest water.
Southwest	Connected to three major inflowing rivers, it serves as a transitional zone dominated by planktonic plants and submerged vegetation
East	The primary outflow of Taihu Lake
East Taihu Bay	A shallow bay primarily utilized for aquaculture and is inhabited by submerged vegetation

2.2. Data

2.2.1. Satellite Data

The Moderate-Resolution Imaging Spectroradiometer (MODIS), onboard Terra and Aqua satellites, has been systematically acquiring extensive datasets in land, atmospheric, and oceanic remote sensing since the first launch of Terra in December 1999. The data used in this study is the level 3 product of MODIS, namely the MOD13Q1 "https://modis.gsfc.nasa.gov/ (accessed on 8 October 2023)". This product integrates observations gathered over a 16-day period from both Terra and Aqua satellites. Following rigorous radiometric and atmospheric correction, the aggregated data is derived using the maximum value composition or constrained view maximum composition method [48]. While the processed data exhibits a reduced temporal resolution, it ensures a close approximation to the authentic values within that timeframe. For a more comprehensive understanding of MOD13Q1's algorithms and data structure, detailed explanations are available at the following website: "https://lpdaac.usgs.gov/products/mod13q1v006/ (accessed on 6 November 2023)".

In our approach to extracting cyanobacterial blooms, we opted for the enhanced vegetation index (EVI) [49,50]. As elucidated by Xiao et al. [51], the coefficients in the fitting formulas for various vegetation indices (ratio vegetation index, normalized difference vegetation index, floating algae index, kernel object space convolution, and object space affine brightness index) are subject to the influence of aerosol optical thickness (AOT). EVI displays the least sensitivity to AOT in relation to unit area biomass. Under conditions of elevated unit area algal biomass, EVI manifests noteworthy variations. Additionally, MODIS's EVI product employs the constrained view angle–maximum value composite algorithm, which significantly enhances pixel utilization. Consequently, this study selected the EVI product from MOD13Q1 to infer the spatiotemporal distribution of cyanobacteria during outbreaks in Taihu Lake. The EVI calculation formula is as follows:

$$EVI = 2.5 \times \frac{\rho_{NIR} - \rho_{RED}}{\rho_{NIR} + C1 \times \rho_{RED} - C2 \times \rho_{BLUE} + L} \quad (1)$$

where, ρ_{NIR} represents the reflectance in the near-infrared band, ρ_{RED} denotes the reflectance in the redlight band, and ρ_{BLUE} corresponds to the reflectance in the blue light band. $C1$ is an atmospheric correction parameter for red light with a numerical value of 6, while $C2$ is the atmospheric correction parameter for blue light with a value of 7.5. L is a soil background adjustment parameter with a numerical value of 1.0. The EVI ranges from -1 to 1, and a threshold of 0 is selected to determine the presence of cyanobacterial blooms. A higher EVI value indicates a higher chlorophyll content [51].

The MOD13Q1 data for the years 2001–2020 was obtained for this study. To ensure data quality, invalid values resulting from cloud interference were eliminated to ensure the EVI values fell within the range of -0.2 to 1.

2.2.2. Meteorological Data

Following prior research, meteorological factors exert significant influence on algal blooms, including temperature, wind, precipitation, and solar radiation. The precipitation (PRE) and near-surface air temperature (T2) data utilized in this study are sourced from the China 1 km Monthly Resolution Precipitation Dataset for the years 1901–2022 "http://www.geodata.cn/data/datadetails.html?dataguid=192891852410344&docid=941 (accessed on 16 November 2023)" and the China 1 km Monthly Resolution Average Temperature Dataset for the years 1901–2022 "http://www.geodata.cn/data/datadetails.html?dataguid=164304785536614&docid=946 (accessed on 16 November 2023)" from the National Earth System Science Data Center, National Science & Technology Infrastructure of China "http://www.geodata.cn (accessed on 16 November 2023)". These datasets are derived from grid data obtained through the Delta downscaling method based on global 0.5° climate data from CRU (Climatic Research Unit) and high-resolution climate data from WorldClim. Data quality is controlled by 496 independent meteorological observation points, including three points in the vicinity of Taihu Lake. The temporal coverage spans from 2001 to 2022, with a spatial resolution of 1 km [52].

Wind at 10 m height above the ground level (wind speed and wind direction are short for WS10&WD10, respectively), and surface solar radiation downwards (SSRD) are sourced from the European Centre for Medium-Range Weather Forecasts (ECMWF) Fifth-Generation Atmospheric Reanalysis Data (ERA5), with a spatial resolution of $0.1^\circ \times 0.1^\circ$.

2.2.3. Cyanobacteria-Emission-Related Data

Drawing on literature research [53], this study obtained the composition and relative proportions of VOCs released by algae at different growth stages, as shown in Table 2. VOC composition was determined through laboratory offline GC-FID/MS measurements, conducted during the stable, senescent, and post-death phases of three typical algae life stages [53]. As algae grow, the relative content of alkenes and oxygenated VOCs (OVOCs) in the released VOCs gradually decreases, while alkanes and volatile sulfur organic compounds (VSOCs) show an increasing trend. The study period is chosen during the rising and relatively stable period of algal blooms from May to October [51,54], focusing solely on VOCs released during the stable period.

The emission rate of VOCs is derived from a meticulous estimation of non-methane total hydrocarbon emission rates as reported in the literature [53]. Yu et al. [53] conducted site measurements, including the VOC emission rates and cyanobacterial cell densities at the sampling points using static chambers. Utilizing empirical data, we posit a proportionality between the release of non-methane total hydrocarbons and algal density. Given an area of approximately 63.2 km^2 of the Zhushan Bay region in Taihu Lake, the VOCs emission rate, and the algal density given by [53], the emission rate of VOCs attributable to algal proliferation during July 2019 was conservatively estimated to range between 0.36 and 0.42 tons per day.

Our postulation encompasses the notion that the VOC content released during the stable phase of algal blooms exhibits a linear augmentation in tandem with the escalating cyanobacterial biomass concentration. The latter, in turn, is posited to be directly proportional to chlorophyll concentration. Furthermore, chlorophyll concentration demonstrates a positive correlation with various vegetation indices, including the EVI, within a defined interval.

Upon ascertaining the VOC release rate emanating from algal blooms in ZhuShan Bay, we integrated this information with the July 2019 distribution of algal blooms in Taihu Lake obtained through MODIS data inversion. Leveraging the distribution and magnitude of EVI values in Taihu Lake during July 2019, we extrapolated the VOC emission quantities for the remaining months of that year. Analogously, we extended this analysis to calculate the aggregate VOCs released from cyanobacterial water blooms in Taihu Lake spanning the years 2001 to 2020.

Table 2. Released VOC components and relative proportions during the stable phase, senescence phase, and apoptosis phase.

Category	VOCs Components	Relative Proportion of Stable Periods	Relative Proportion of Senescence	Relative Proportion of Apoptotic Phase
Alkanes	ETHANE CH_3CH_3	0.0414	0.0461	0.0434
	Propane C_3H_8	0.0494	0.0703	0.0578
	ISOBUTANE C_4H_{10}	0.0317	0.0419	0.0343
	n-Butane C_4H_{10}	0.0422	0.0389	0.0327
	Cyclopentane C_5H_{10}	0.0486	0.0259	0.0166
	2-Methylbutane C_5H_{12}	0.0584	0.0401	0.0327
	Pentane C_5H_{12}	0.0622	0.0486	0.0473
	2,2-Dimethylbutane C_6H_{14}	0.0113	0.0078	0.0000
	3-METHYLPENTANE C_6H_{14}	0.0286	0.0235	0.0540
	Heptane C_7H_{16}	0.0249	0.0320	0.0385
	N-NONANE C_9H_{20}	0.0301	0.0350	0.0205
Alkenes	ETHYLENE C_2H_4	0.0622	0.0498	0.0368
	PROPYLENE C_3H_6	0.0494	0.0473	0.0412
	2-BUTENE C_4H_8	0.0188	0.0115	0.0138
	1-BUTENE C_4H_8	0.0339	0.0199	0.0188
	CIS-2-BUTENE C_4H_8	0.0181	0.0386	0.0111
	1,3-Butadiene C_4H_6	0.0098	0.0048	0.0133
	1-Pentene C_5H_{10}	0.0301	0.0181	0.0243
	trans-2-Pentene C_5H_{10}	0.0128	0.0109	0.0188
	Isoprene C_5H_8	0.0870	0.0395	0.0327
	CIS-2-PENTENE C_5H_{10}	0.0249	0.0103	0.0155
	1-Hexene C_6H_{12}	0.0279	0.0139	0.0440
OVOCs	Acrolein C_3H_4O	0.0264	0.0476	0.0166
	Acetone C_3H_6O	0.0795	0.0576	0.0407
	2-Butanone C_4H_8O	0.0430	0.0350	0.0473
VSOCs	Carbon disulfide CS_2	0.0475	0.0157	0.0445
	Dimethyl sulfide C_2H_6S	0.0000	0.0350	0.0232
	1,1′-Thiobisethane $C_4H_{10}S$	0.0000	0.0455	0.0457
	Dimethyl disulfide $C_2H_6S_2$	0.0000	0.0259	0.0368
	Methyl propyl disulfide $C_4H_{10}S_2$	0.0000	0.0407	0.0490
	Dimethyl trisulfide $C_2H_6S_3$	0.0000	0.0000	0.0183
	ISOPROPYL DISULFIDE $C_6H_{14}S_2$	0.0000	0.0223	0.0299

2.2.4. Machine Learning Model and SHapley Additive exPlanations (SHAP) Approach

In order to determine the relative importance of various meteorological factors on algal blooms and the release of VOCs associated with these blooms, we utilized machine learning methods. The Light Gradient Boosting Machine (LightGBM) is a gradient-boosting framework utilizing tree-based learning algorithms [55]. Traditional implementations of gradient-boosting decision trees face challenges in balancing accuracy and efficiency, particularly with high feature dimensions and large datasets. To address this, LightGBM incorporates gradient-based one-side sampling and exclusive feature bundling, reducing training time and memory usage while maintaining accuracy [55,56]. In this study, the LightGBM model is employed to simulate the impact of meteorological factors on cyanobacterial blooms using the EVI values and corresponding meteorological factors. Each lake area is individually modeled for independence. Invalid values (EVI < 0) are filtered, and data is randomly split (80% training, 20% testing). Functions "extra trees" and "early stop rounds" of LightGBM were used to prevent overfitting.

In this study, the SHAP approach was employed to measure the impact of input features on the final model simulation, utilizing coalitional game theory. In essence, the contribution of each input feature is determined through its marginal impact. For a simulated sample x_i with K input features producing a simulated value $f(x_i)$ at a given

time, the explanatory model f is expressed as a linear function of feature attribution (Equation (2)).

$$f(x_i) = \varnothing_o(f, x) + \sum_{j=1}^{K} \varnothing_j(f, x_i) \quad (2)$$

where $\varnothing_j(f, x_i)$ is the SHAP value representing the contribution of input feature j on the simulation of model f for the simulated sample x_i. The base value, $\varnothing_o(f, x)$ = E [$f(x)$], is the expected value of the model output over the data set.

The SHAP value $\varnothing_j(f, x)$ is the weighted average of $\varnothing_j$ values across all possible feature subset combinations.

$$\varnothing_j(f, x) = \sum_{S \subseteq K \setminus \{j\}} \frac{|S|!(K-|S|-1)!}{K!} [f_x(S \cup \{j\}) - f_x(S)] \quad (3)$$

where $S \subseteq \{0, 1\}^K$ and K is the set of all K input features. $|S|$ is the cardinality of the set S or the number of elements in the set S.

Here, if $\varnothing_j(f, x) > 0$ (or <0), it refers to the positive (negative) effect of the feature j that increases (decreases) the simulation above (below) the base value. The higher the absolute SHAP value of the input feature, the more distinct the impact of that feature on the model simulations.

3. Results

3.1. Long-Term Spatiotemporal Characteristics of EVI

Figure 2 illustrates the multi-year temporal and spatial variations in annual mean cyanobacterial-bloom-associated EVI from 2001 to 2020. Significant interannual variations in the coverage of cyanobacterial blooms can be observed during the 20 years, indicating strong variations in affecting factors. Overall, cyanobacterial blooms in Taihu Lake were not particularly severe in the early 21st century (first row in Figure 2). However, cyanobacterial blooms in Taihu Lake became significantly worse starting in 2006. Examining the distribution of EVI during the annual bloom periods on the grid, from 2001 to 2005, blooms were mainly concentrated in Zhushan Bay in the northern part of Taihu Lake, as well as in Meiliang Bay. East Taihu Bay is dominated by aquatic vegetation, resulting in consistently high EVI levels.

Starting in 2006, there was a sudden increase in the coverage of cyanobacterial blooms. During these two years, Taihu Lake as a whole experienced a severe level of cyanobacterial blooms, coinciding with the water crisis affecting millions of people in Wuxi in 2007. After 2008, the coverage of blooms decreased, and by 2011, it had returned to the levels seen before 2006. In the decade from 2011 to 2020, the Northwest and Meiliang Bay were consistently covered by cyanobacterial blooms. By 2020, these two areas were almost completely covered and approximately two-thirds of the central region experienced cyanobacterial-bloom coverage. The southwestern region had relatively low coverage in 2014, but in other years, it was comparable to the levels seen in 2006 and 2007. In 2019 and 2020, the coverage reached a significant extent.

In summary, the coverage of cyanobacterial blooms in Taihu Lake from 2001 to 2020 exhibits an M-shaped trend with two peaks. The first peak occurred in 2006 and 2007, followed by a slow decrease. However, the reduction was not substantial, and after 2011, there was an upward trend again, reaching the second peak in 2020, which is the highest in 20 years. This trend aligns with the findings of other scholars [57].

We further compared the annual mean EVI values, the annual averaged number of grids that are covered with cyanobacterial blooms, and the month of maximum EVI of Taihu Lake and its five subregions (Northwest, Meiliang Bay, Gonghu Bay, Central, Southwest) from 2001 to 2020.

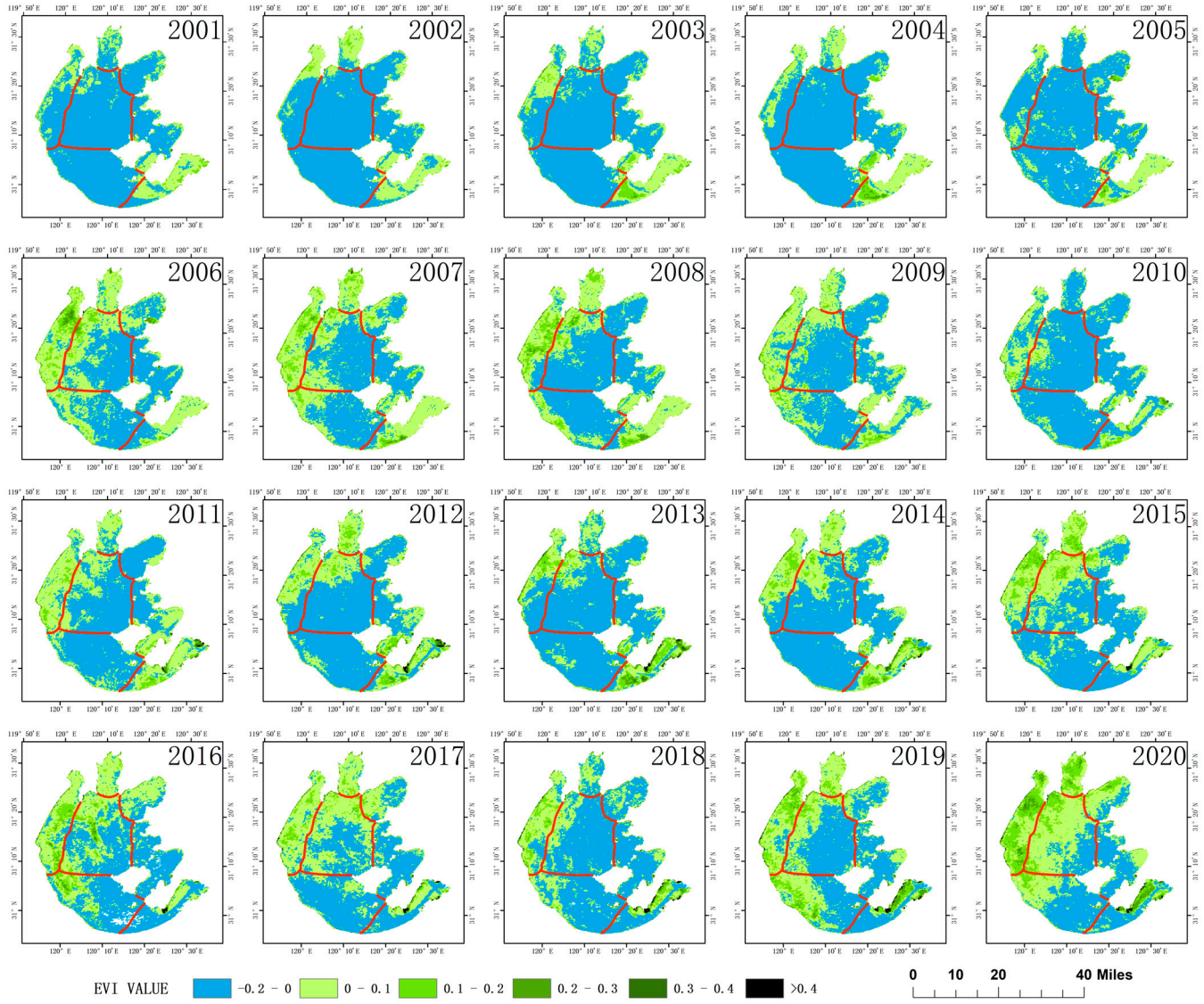

Figure 2. Annual average EVI distribution in Taihu Lake from 2001 to 2020 (Red line marks the boundary of the subareas shown in Figure 1).

The fitting curve of the annual mean EVI in Figure 3a shows an increasing trend from 2001 to 2020, with the average EVI values consistently below 0.12 in Taihu Lake. The year 2006 witnessed the most rapid increase, and although there were slight decreases in the subsequent years, they did not return to the levels before 2003. In 2019, Taihu Lake reached its maximum average EVI value. This suggests that despite efforts to control and mitigate cyanobacterial blooms, Taihu Lake has not eliminated the increasing trend of cyanobacterial blooms. The number of grid cells covered by cyanobacterial blooms in Taihu Lake was below 1.05×10^4 (22.7% of the Taihu Lake area) before 2005. It surged to around 1.6×10^4 (monthly average coverage area of 35.8%) in 2006, with a slight increase in 2007. In the following three years, the coverage area of blooms continued to decrease, indicating the apparent effectiveness of artificial intervention. By 2010, the coverage area had even returned to the 2005 level. However, the subsequent years witnessed fluctuations, persisting until 2020 when the coverage area reached its 20-year peak, with approximately 2.01×10^4 grids (monthly average coverage area of 46.8%) covered by cyanobacterial blooms.

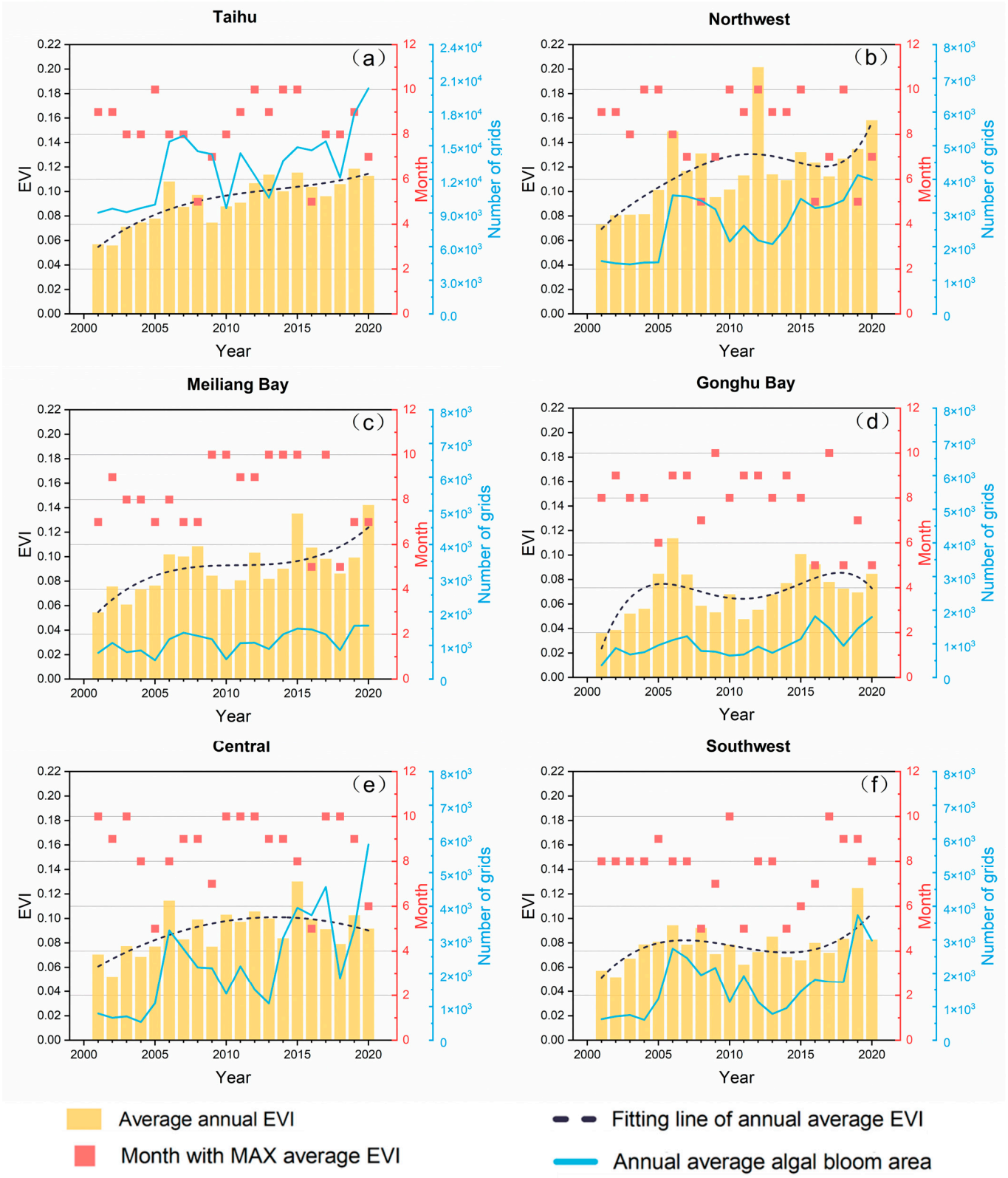

Figure 3. Temporal evolution of annual mean EVI (yellow bars) along with its fitting curve (black dashed lines), the annual averaged no. of grids that are covered by cyanobacterial blooms (light blue solid lines), and month of maximum EVI (red squares) in Taihu Lake (**a**) and its subregions (**b**–**f**), representing the Northwest, Meiliang Bay, the Gonghu Bay, the Central, and the Southwest, respectively.

In terms of each subregion of Taihu Lake, it can be observed that, except for the Central region, the annual mean EVI in each subregion shows an upward trend. However, the variability in EVI, and the years with the highest average EVIs, exhibit notable differences among the regions. Based on the bar charts and their fitted curves, Northwest, Meiliang Bay, and Southwest display a unimodal trend characterized by an initial increase, followed by a decrease, and then another increase. Gonghu Bay exhibits a bimodal trend, while Central shows a unimodal variation. Figure 3 also reveals that the annual average number of grids of algal blooms from May to October each year is generally consistent with the overall EVI trends, with some exceptions. For example, in Figure 3e, although the average EVI level for Central in 2020 was not the highest in recent years, the annual average grid coverage of algal blooms in the Central area was the highest in 20 years, covering approximately 46.5% of the lake area. The months with the most severe EVI values are September and October, followed by July, August, and May. The relatively low frequency of peak EVI in June may be associated with the Meiyu System in Jiangsu province, which is characterized by large rainfall.

Significant disparities are also evident in the average EVI values among the lake regions. Northwest, with the highest average EVI level, surpassed 0.07 in 2001, and doubled to 0.149 in 2006, surpassing all other regions during that period. In 2012, Northwest's average EVI further rose to around 0.2, two to three times higher than the average EVI of other regions during the same period. Conversely, Gonghu Bay, with the lowest average EVI level, had an average EVI of only 0.036 in 2001. Its two peak values occurred in 2006 (0.114) and 2015 (0.101).

Based on the above analysis, ranking the severity of algal blooms in the five subregions relative to Taihu Lake as a whole, the order is Northwest > Meiliang Bay > Central > Southwest > Gonghu Bay. The seasonal threat level is roughly similar between summer and autumn but is greater than in spring.

3.2. Impacts of Meteorological Factors

3.2.1. The Spatiotemporal Variations of Meteorological Factors

In the context of global warming, meteorological factors that significantly influence algal-bloom growth have undergone changes. Based on prior research, we have selected T2, precipitation, WS10, WD10, and SSRD as the key variables for our investigation due to their discernible impacts on algal-bloom development. Figure 4 illustrates the variations in WS10, SSRD, T2, and precipitation in Taihu Lake from 2001 to 2020.

The trends in variations of SSRD and T2 exhibit a notable consistency. This observation aligns with our common understanding that solar radiation serves as the primary source of energy. Years with severe cyanobacterial blooms align predominantly with periods of elevated temperatures (The average from 2001–2005 was 23.82°, the average in 2006, 2007, 2019, and 2020 was 24.24°). The significant algal-bloom events in 2006 and 2007 coincided with a gradual warming trend since the early 21st century, with the annual average temperature reaching a peak in 2007, underscoring the irreplaceable role of climate-induced warming in the occurrence of large-scale cyanobacterial blooms. Similarly, the sustained warming trend post-2014 may contribute to the substantial increase in cyanobacterial-bloom areas in recent years.

Due to the vast expanse of Taihu Lake, diverse water movements, and variations in depth, coupled with urban heat island effects, temperature disparities across different regions of the lake are evident. Using the year 2020, characterized by the highest VOC emissions, as an example, as shown in Figure 5a,c, it is evident that temperatures near the lake shore are notably higher than those in the distant offshore areas, sometimes exceeding a difference of 1 degree Celsius. In contrast, solar radiation variations in the Taihu Lake region are not as pronounced. When considering factors excluding nutrient enrichment, the relatively higher temperatures near the lake shore to some extent account for the increased algal density in these areas. The multi-year annual precipitation in Taihu Lake exhibits notable fluctuations. The minimal precipitation occurred in 2003 and 2004, with

monthly precipitation falling below 90 mm from May to October. In contrast, the zenith of precipitation was recorded in 2020, reaching 161 mm per month. Despite the paucity of precipitation in 2003 and 2004, no widespread algal blooms were observed, whereas 2020 witnessed the onset of severe algal-bloom events. This indicates that, to some extent, increased precipitation promotes the spread of algal blooms. For instance, the years 2001 and 2002 experienced more rainfall than 2006 and 2007, yet the algal-bloom situations were reversed. We speculate that this discrepancy may be related to the spatial distribution of rainfall. If rainfall is more prevalent upstream, it could accelerate the accumulation of nutrient-rich substances from upstream into the lake, creating favorable conditions for algal-bloom outbreaks. Conversely, it may lead to an increase in lake-water levels, disrupting nutrient-rich conditions, lowering water temperatures, and weakening photosynthesis due to reduced solar radiation, coupled with increased wind strength—factors that are unfavorable for algal growth. The spatial distribution of precipitation in Taihu Lake during 2020 is depicted in Figure 5b. It is discerned that the southwest region experiences higher precipitation, while the southeast region encounters lower precipitation. The rainfall distribution in 2003 and 2004 closely resembles that of 2020. However, even from the perspective of spatial distribution, disentangling the relationship between precipitation patterns and the occurrence of algal blooms remains challenging.

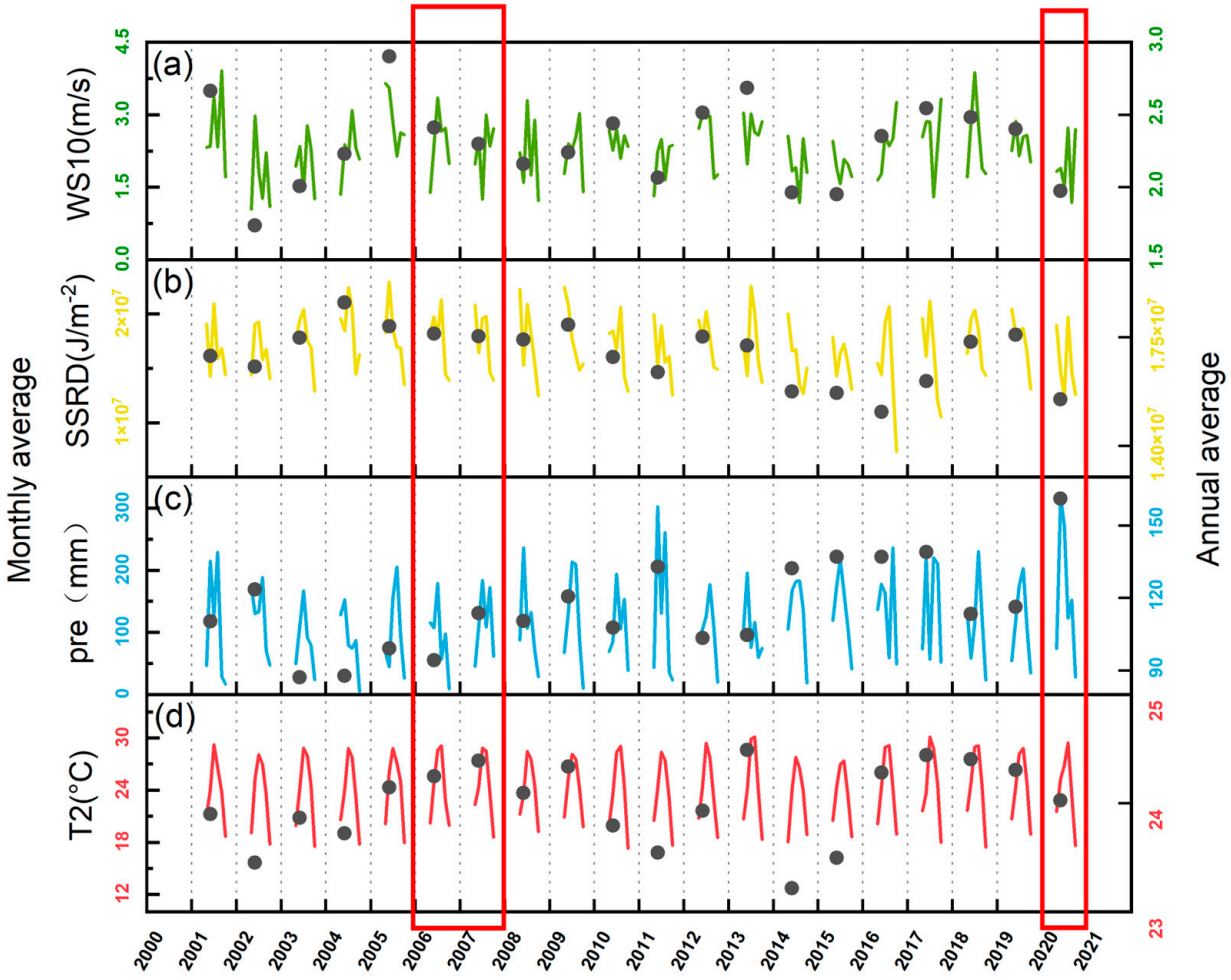

Figure 4. Time series of monthly (lines) and annual (black solid dots) mean WS10 (**a**), SSRD (**b**), T2 (**d**), and monthly and annual accumulated precipitation (**c**) in the Taihu Lake region from 2001 to 2020.

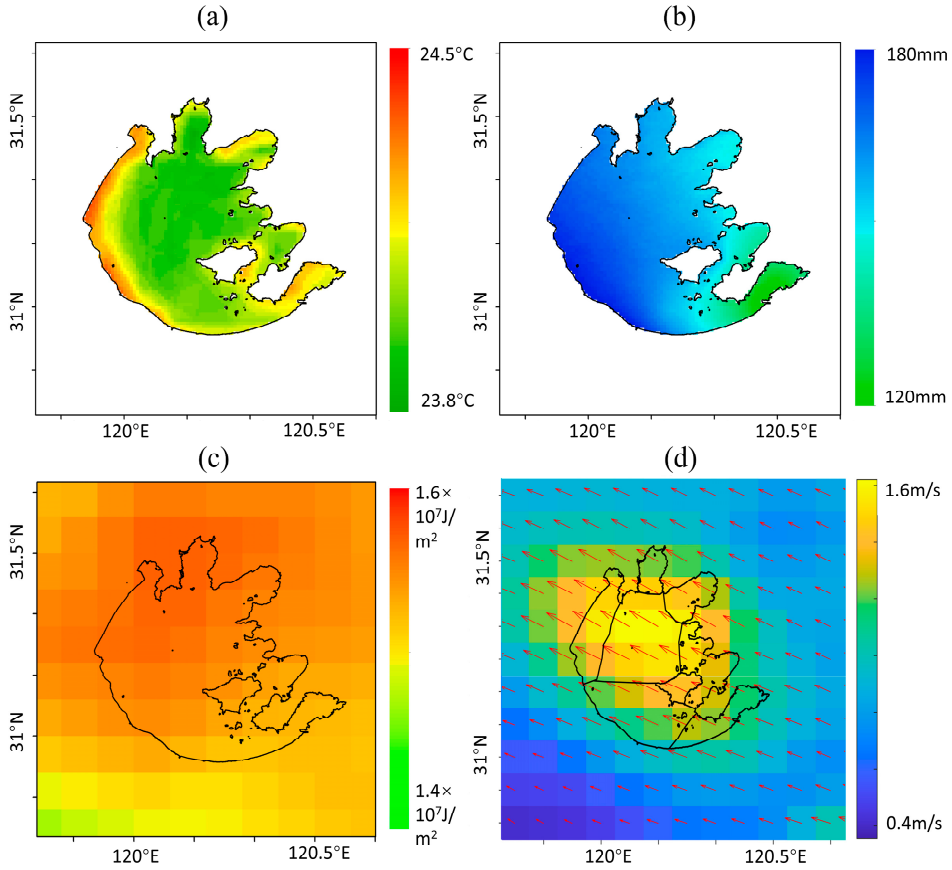

Figure 5. Annual average T2 (**a**), pre (**b**), SSRD (**c**), and wind field (**d**) diagram of Taihu Lake in 2020.

The multi-year wind speed presented in Figure 4 indicates a relatively stable pattern. The annual average wind speed primarily oscillates within the range of 2–3 m/s. The dominant wind directions in Taihu Lake from May to October are illustrated in Figure 5d. During this period, the prevailing wind direction is east-southeast, with relatively low average wind speeds. This pattern facilitates the accumulation of cyanobacterial blooms towards the northwest shore of Taihu Lake. The central region of the lake, being more open without topographical obstacles, experiences higher wind speeds compared to the shoreline. This phenomenon contributes, to some extent, to the heightened occurrence of cyanobacterial blooms in the Northwest, Meiliang Bay, and Southwest regions of Taihu Lake.

3.2.2. The Relative Importance of Meteorological Factors

The aforementioned analysis underscores the interplay of various meteorological factors in influencing cyanobacterial blooms. However, these insights are contingent upon controlling variables. In the actual Taihu Lake ecosystem, the formation of cyanobacterial blooms is intricately linked to these meteorological factors, making it impractical to consider individual variables. The relative importance of each meteorological factor is seldom explored in existing research and is challenging to determine. Consequently, it is necessary to further elucidate the relative importance of each meteorological factor.

Modeling was conducted for each region. Figure 6 illustrates the influence of various meteorological factors on EVI values based on the SHAP method in different lake regions of Taihu Lake. We observed that, across all lake regions, T2 has the highest sensitivity to the severity of cyanobacterial blooms (EVI values), accounting for over 30% of the total contribution. The sensitivity of rainfall remains relatively stable. The contribution of wind speed is consistently 4–7% lower in the two western lake regions, Northwest and Southwest, in comparison to other lake regions. We hypothesize that this discrepancy may be attributed to the hindered transport of algae to other areas by wind. Interestingly, in

Meiliang Bay, where there is minimal SSRD, a distinct low sensitivity is observed. However, at present, a comprehensive and scientifically sound explanation for this phenomenon remains elusive.

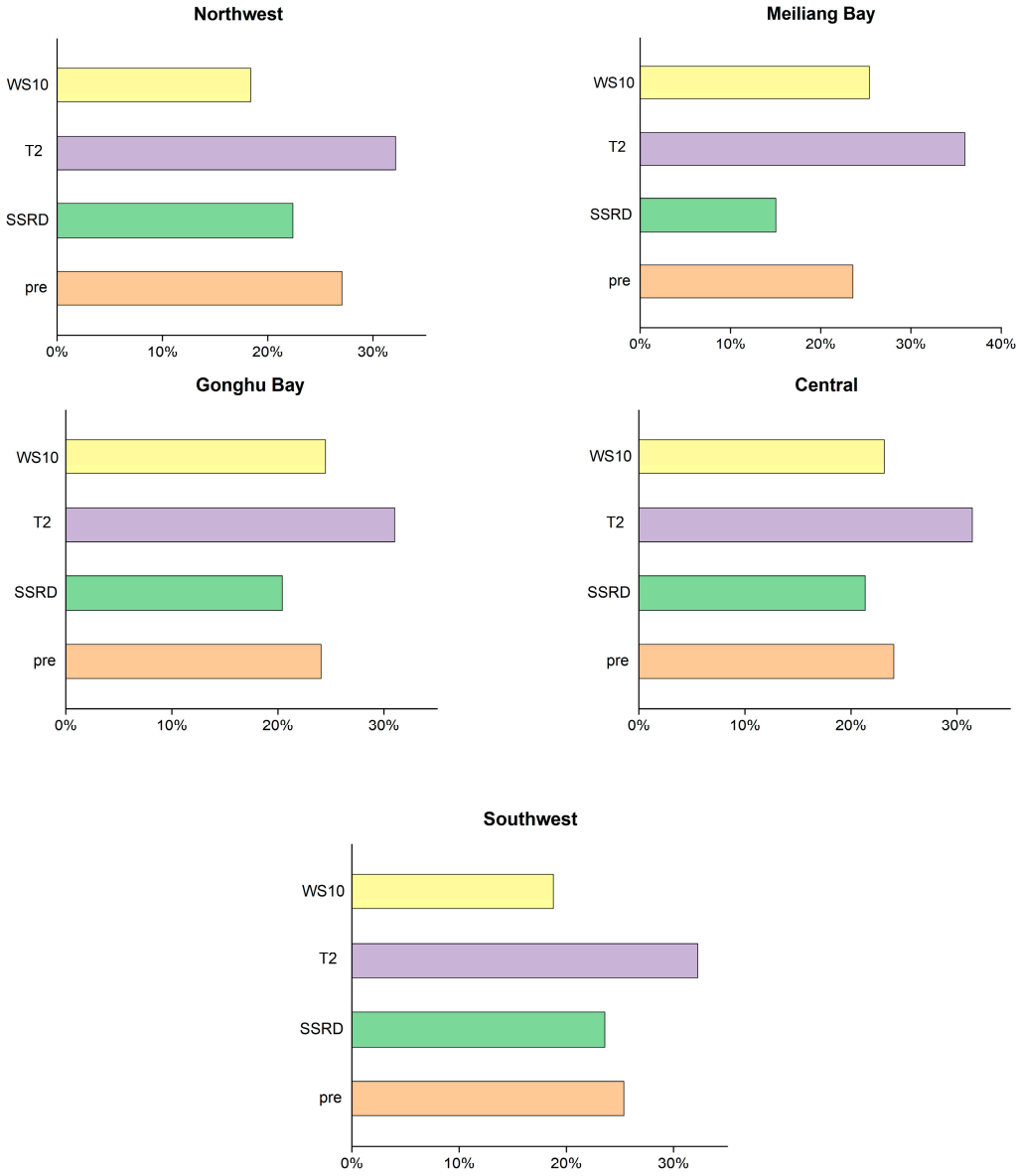

Figure 6. Sensitivity of EVI values to various meteorological factors in each subregion.

To better comprehend the impact of meteorological elements on the generation of cyanobacterial blooms, we examined the SHAP values for Taihu Lake concerning the variations in meteorological elements. As shown in Figure 7, in Taihu Lake, only temperature exhibits a distinct linear trend, with the inflection point at 20.5 °C where temperatures below hinder cyanobacterial growth, while those above favor it. Precipitation does not show clear relationships, but it can be observed that monthly precipitation exceeding 250 mm significantly increases the SHAP values of precipitation, indicating an increase in EVI values and consequently higher cyanobacterial concentrations. Similarly, an increase in SSRD values enlarges cyanobacterial concentrations, though it does not necessarily increase the bloom area. In terms of monthly mean wind speed, the SHAP values visibly decrease when the wind speed exceeds approximately 3 m/s.

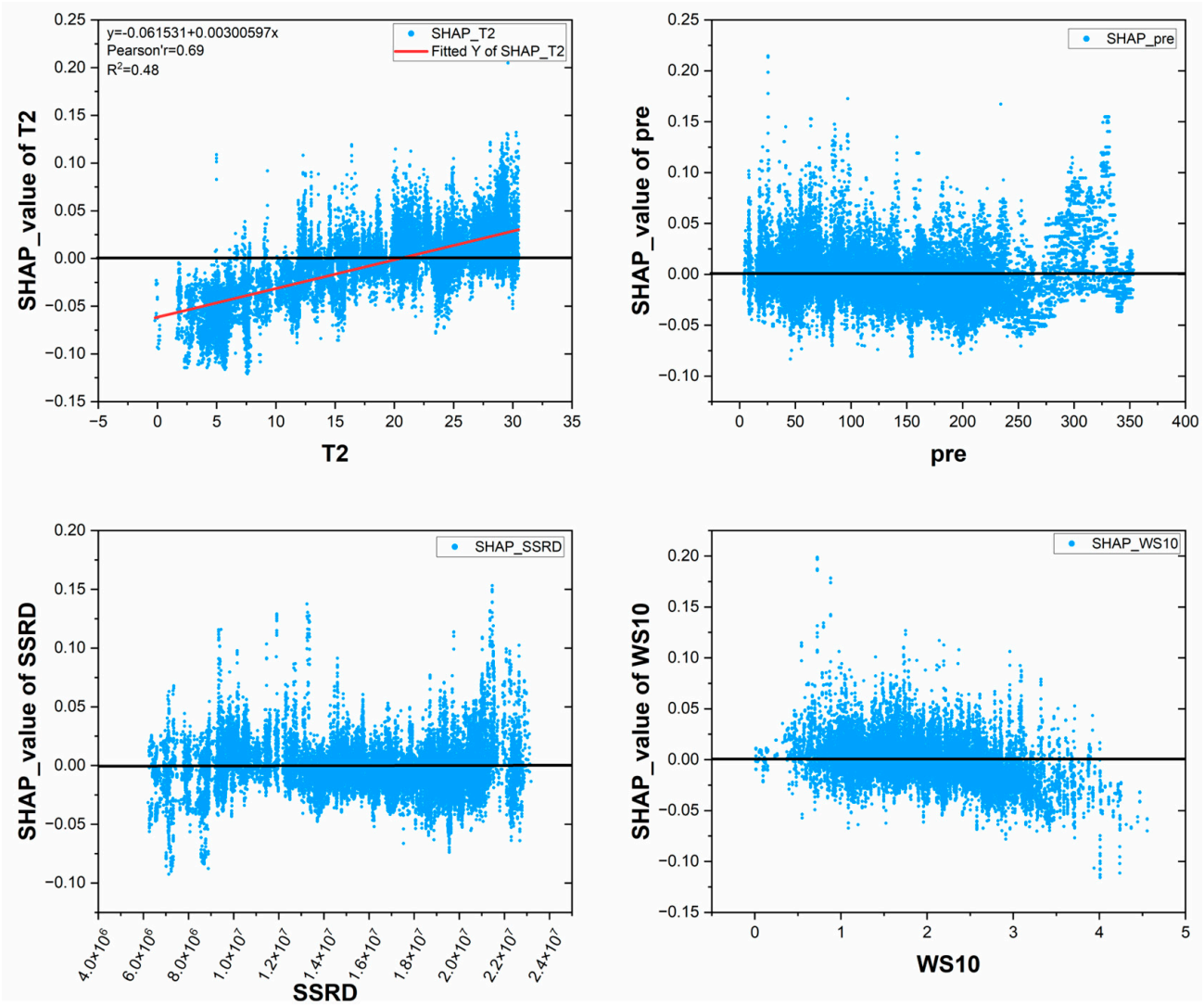

Figure 7. The relative relationship between various meteorological factors and SHAP values for the entire Taihu Lake.

3.3. Spatiotemporal Characteristics of Retrieved VOCs Emission

In accordance with the data introduced earlier, the emission rate of VOCs in Taihu Lake was determined. Our calculations exclusively consider the months from May to October. Figure 8 illustrates the estimated annual maximum aggregate emissions of VOCs associated with cyanobacterial blooms in Taihu Lake, as well as the range of emissions of each grid (illustrated as a boxplot), during the period 2001–2020.

The trends in the overall VOC emission from cyanobacterial blooms exhibit a fluctuating increasing pattern. In the year 2001, the maximum estimated amount of VOC content released from Taihu Lake's cyanobacterial blooms was 347,523.5 kg. A significant surge occurred in 2006 and 2007, resulting in a nearly threefold increase in the total VOC emission. A consistent decline in VOC emissions was observed from 2006 to 2010. Notably, around 2018, the VOCs released from cyanobacterial blooms in Taihu Lake rebounded to levels reminiscent of a decade earlier but with larger variations. In 2020, the total VOC emission from cyanobacterial blooms in Taihu Lake was 5.35 times higher than that in 2001 and 1.71 times higher than that in 2006. We also calculated the biogenic and anthropogenic VOC emissions of the surrounding cities of Taihu Lake to investigate the potential impact of the VOCs emitted from Taihu Lake in July 2019. The biogenic VOC emissions were calculated using the Model of Emissions of Gases and Aerosols from Nature (MEGAN v2.1) coupled

with the Weather Research and Forecasting (WRF) system [58] and the anthropogenic VOC emissions were derived from the Multi-resolution Emission Inventory model for Climate and Air Pollution Research (MEIC v1.4) [59,60]. In July 2019, the VOCs emitted by Taihu algal blooms (212 t) were approximately 11% of the natural VOC emissions (1923 t) and 1.6% of the anthropogenic emissions (13,108 t) within the 10 km outside Taihu Lake. In the northwestern region of Taihu, where algal-bloom activity is more frequent and severe, the VOCs from algal blooms over the northwestern of Taihu reached 29.9% of the surrounding natural sources (386 t) and 3.2% of the anthropogenic sources (3565 t). Such results indicate that VOCs from algal blooms cannot be ignored.

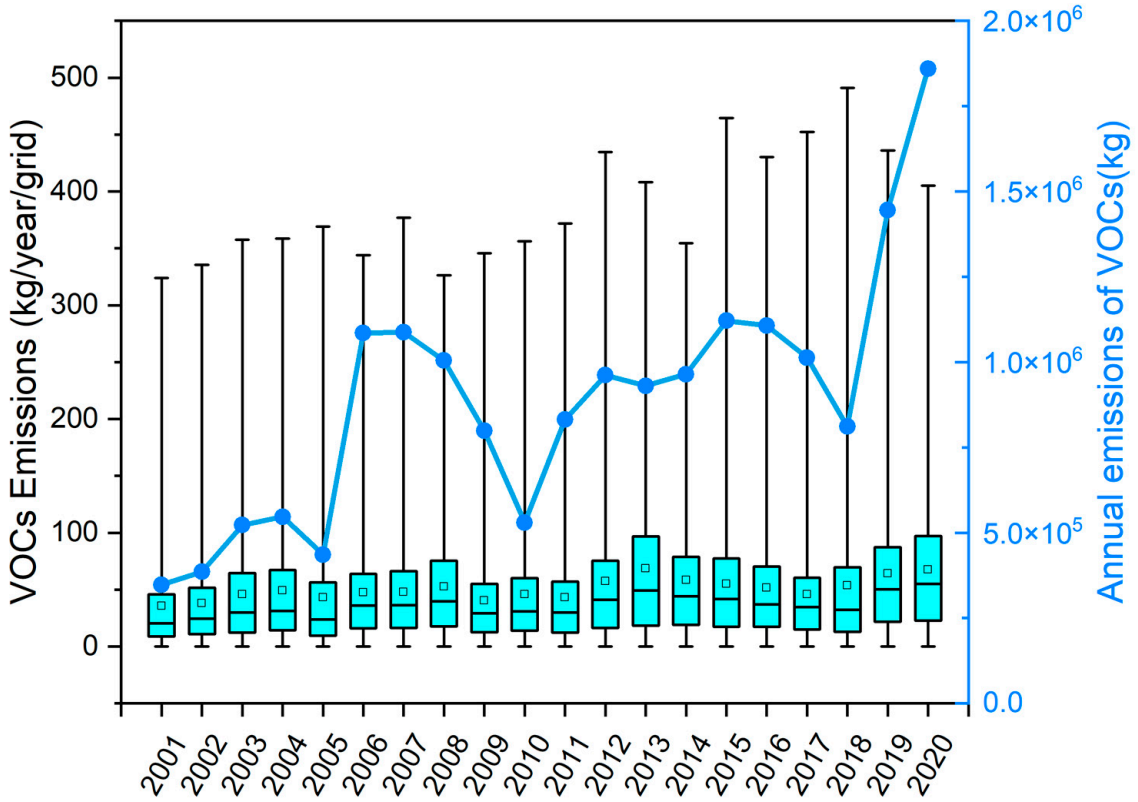

Figure 8. Boxplot of emissions of VOCs of each grid and line chart of annual VOC emissions in Taihu Lake from 2001 to 2020. The line and square in the boxplot represent the median and mean values, respectively.

According to Table 2, we observe that isoprene is the organic compound with the highest release proportion during the stable phase of algal blooms. It is also the most abundant non-methane volatile organic compound emitted globally, exhibiting strong reactivity in atmospheric chemical reactions. Isoprene serves as a primary precursor to secondary organic aerosols and ozone on a global scale [61]. Figure 9 illustrates the spatial distribution of estimated isoprene released during cyanobacterial blooms in Taihu Lake over multiple years based on the proportion of isoprene given by Table 2 and the spatial distribution of EVI.

East Taihu Lake Bay, characterized by perennial aquatic vegetation cover, consistently exhibits higher EVI values, resulting in larger emission amounts each year. Figure 9 clearly indicates that the western and northern regions of Taihu Lake are considerably more affected than the eastern and southern regions. The most pronounced release of isoprene from cyanobacterial blooms occurred in 2020, with the highest emission point located at the outlet of Zhushan Bay in the Northwest region, at a certain distance from the shore, as well as in the northeastern region of Meiliang Bay and a small part of the northern region of Gonghu Bay. This emission pattern shows a tendency to spread toward Central.

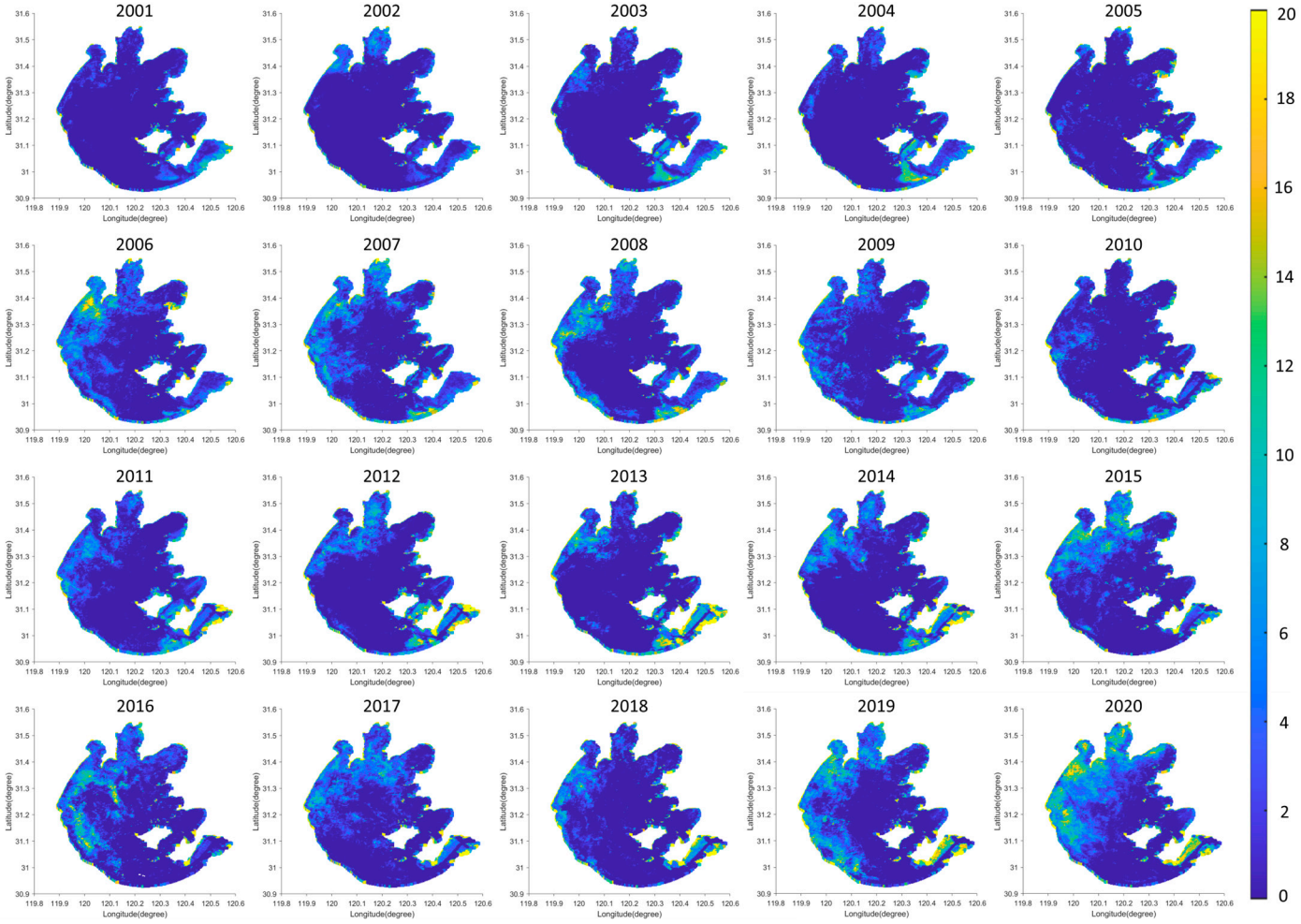

Figure 9. Spatial distribution of estimated isoprene emissions (kg) from cyanobacterial blooms in Taihu Lake from 2001 to 2020.

From 2001 to 2005, isoprene emissions were mainly concentrated in Zhushan Bay in the Northwest and Meiliang Bay, predominantly near the shore. In 2006, the widespread outbreak of cyanobacterial blooms led to a sharp increase in VOC emissions, with the most affected areas being the Northwest, the northern part of Meiliang Bay, and the coastal areas in the eastern and southern parts of Gonghu Bay. After 2011, emissions from the western region and Meiliang Bay began to increase again, reaching another high-value year similar to 2006. The emissions continued to approach the Southwest and Central regions, and there was no sustained decrease similar to the post-2006 period. Conversely, a notable upsurge persisted in 2019 and culminated in 2020, where almost half of Taihu Lake was shrouded in cyanobacterial blooms. The release of isoprene from these blooms, surpassing the threshold of 10 kg per grid annually, exerts discernible impacts on both the ecological milieu of Taihu Lake and the surrounding atmospheric environment.

4. Discussion

The causes of cyanobacterial blooms, the mechanisms influencing their growth, the resulting harm, and preventive measures have garnered significant attention. However, recent findings from the retrospective inversion of algal blooms in Taihu Lake underscore the need for further research into this phenomenon. Climate change, a factor leading to increased instability in Taihu Lake's cyanobacterial blooms, especially in the context of a stable nitrogen–phosphorus ratio, is identified as one contributing factor. Statistical results on the climate conditions in Taihu Lake from this study show that algal-bloom disasters

in years like 2006 and 2007 were indeed associated with abnormal temperature increases and changes in solar radiation, promoting the occurrence of algal blooms. Additionally, the emission of VOCs during these years was high, posing a significant threat to the air quality in nearby cities. Meteorological factors intertwine with various elements, making it challenging to determine their impact on cyanobacterial blooms. Interpretable machine learning reveals the relative importance of meteorological factors, aiding our understanding of lake dynamics and ecological mechanisms.

Furthermore, our focus on the harm caused by cyanobacterial blooms in Taihu Lake has shifted to the VOCs they release, which have not been comprehensively studied. Recent studies indicate that these VOCs, acting as precursors, can impact ozone levels in large water bodies and adjacent urban areas, indirectly affecting the atmospheric environment. Existing methods for estimating VOCs rely on experiments or online instruments, limited to small-scale applications. This study addresses this limitation by establishing a relationship between algal blooms and volatile organic compounds, employing satellite remote sensing to indirectly assess the status of these compounds in large water bodies. This approach contributes to estimating the potential threat of ozone outbreaks in large water bodies and their surrounding areas, providing crucial insights for warning against such events. It is worth noting that we assumed the detected aquatic vegetation in Taihu Lake during the cyanobacteria seasons is only cyanobacteria, which could be a source of error. For example, East Taihu Lake is dominated by submerged vegetation which surely have different VOC emission characteristics.

While this approach can be extended to explore the relative importance of other influencing factors, there are limitations to this study. For example, only one vegetation index, the EVI, was used to represent the spatiotemporal-intensity distribution of algal blooms. Other indexes, such as the floating algae index with better representativeness of algal blooms, could be further investigated. Fixed emission ratios were chosen when considering VOC components, yet variations in the types and relative proportions of VOCs released by algal blooms may occur under different growth conditions and stages. It is imperative for future research to clarify the relative proportions of algal blooms at different stages and the types and proportions of VOCs released. Additionally, the low temporal resolution of MODIS product data and potential data gaps may affect the calculation of average EVI, a consideration that should be factored into the interpretation of study results and conclusions. Furthermore, a follow-up study of the impact of the released VOCs on the surrounding atmospheric environment is needed.

5. Conclusions

This study focuses on explaining the extent of meteorological influence on cyanobacterial blooms in Taihu Lake based on a deep-learning approach and attempting to construct an inventory of VOC emissions from these blooms against the backdrop of increasing algal blooms. Using MODIS EVI data from 2001 to 2020, we inferred the spatiotemporal distribution characteristics of cyanobacterial blooms in Taihu Lake. The LightGBM machine learning method and the SHapley Additive exPlanations approach for interpretability were constructed to calculate the relative influence of various meteorological factors on cyanobacterial growth. Based on existing experimental data and satellite remote sensing, we constructed the first inventory of VOC emissions from cyanobacterial blooms in Taihu Lake. This inventory records the distribution of various VOCs released by cyanobacterial blooms in Taihu Lake over the past two decades. The conclusions are as follows:

(1) Cyanobacterial blooms in Taihu Lake are primarily distributed in the Northwest and Meiliang Bay areas, where VOCs are released. The EVI index exhibits a fluctuating upward trend, with explosive growth during the outbreak periods in 2006 and 2007. In 2020, the EVI reached the highest level, 1.71 times that of 2006, indicating a sustained deterioration trend in cyanobacterial blooms in Taihu Lake.

(2) In all regions of Taihu Lake, temperature is the most significant meteorological factor influencing cyanobacterial blooms. Wind speed and direction usually affect the transportation and accumulation of cyanobacterial blooms in the northwestern regions.
(3) Isoprene is the predominant component among the VOCs released by cyanobacterial blooms. The distribution of VOCs closely aligns with the concentration of cyanobacterial blooms, emphasizing the need to pay attention to air pollution, such as ozone increase and aerosol augmentation, in regions where cyanobacterial blooms are concentrated.

Further studies on the impact of the released VOCs on the air quality of the surrounding cities will be carried out using the latest three-dimensional atmospheric transport and chemical models.

Author Contributions: Conceptualization, M.S.; Methodology, Z.L., C.Z. and M.S.; Software, Z.L., S.L. and C.Z.; Validation, S.L.; Formal analysis, Z.L.; Investigation, Z.L. and M.S.; Resources, S.W. and M.S.; Data curation, S.L., C.Z. and S.W.; Writing—original draft, Z.L.; Writing—review & editing, Y.Z., S.W. and M.S.; Visualization, Z.L. and C.Z.; Supervision, M.S.; Project administration, Y.Z. and M.S.; Funding acquisition, Y.Z. and M.S. All authors have read and agreed to the published version of the manuscript.

Funding: This research is supported by funding from the National Natural Science Foundation of China (42307132) and the Special Science and Technology Innovation Program for Carbon Peak and Carbon Neutralization of Jiangsu Province (Grant No. BE2022612).

Data Availability Statement: The MOD13Q1 data is available at: https://modis.gsfc.nasa.gov/; the China 1 km Monthly Resolution Precipitation and Average Temperature Dataset for the years 1901–2022 data are available at: http://www.geodata.cn/data/datadetails.html?dataguid=192891852410344&docid=941 and http://www.geodata.cn/data/datadetails.html?dataguid=164304785536614&docid=946; and the ERA5 data can be accessed at: https://cds.climate.copernicus.eu.

Acknowledgments: The author would like to express sincere gratitude to the European Space Agency for generously providing the ERA5 data, NASA for supplying MODIS product data, and the National Earth System Science Data Center and the National Science & Technology Infrastructure of China for contributing meteorological datasets.

Conflicts of Interest: The Author Suyang Wang was employed by the Shanghai Rural Commercial Bank. The remaining authors declare that the research was conducted in the absence of any commercial or financial relationships that could be construed as a potential conflict of interest. The funders had no role in the design of the study; in the collection, analyses, or interpretation of data; in the writing of the manuscript; or in the decision to publish the results.

References

1. Yang, L.; Yang, X.; Ren, L.; Qian, X.; Xiao, L. Mechanism and control strategy of cyanobacterial bloom in Lake Taihu. *J. Lake Sci.* **2019**, *31*, 18–27.
2. Zhang, Y.; Su, Y.; Liu, Z.; Sun, K.; Kong, L.; Yu, J.; Jin, M. Sedimentary lipid biomarker record of human-induced environmental change during the past century in Lake Changdang, Lake Taihu basin, Eastern China. *Sci. Total Environ.* **2018**, *613–614*, 907–918. [CrossRef] [PubMed]
3. Deng, J.; Wang, Y.; Liu, X.; Hu, W.; Zhu, J.; Zhu, L. Spatial distribution and risk assessment of heavy metals and As pollution in the sediments of a shallow lake. *Environ. Monit. Assess.* **2016**, *188*, 296. [CrossRef] [PubMed]
4. Qin, B.; Zhu, G.; Gao, G.; Zhang, Y.; Li, W.; Paerl, H.W.; Carmichael, W.W. A Drinking Water Crisis in Lake Taihu, China: Linkage to Climatic Variability and Lake Management. *Environ. Manag.* **2009**, *45*, 105–112. [CrossRef] [PubMed]
5. Zuo, Z. Why Algae Release Volatile Organic Compounds—The Emission and Roles. *Front. Microbiol.* **2019**, *10*, 446976. [CrossRef]
6. Li, M.; Zhang, Q.; Zheng, B.; Tong, D.; Lei, Y.; Liu, F.; Hong, C.; Kang, S.; Yan, L.; Zhang, Y.; et al. Persistent growth of anthropogenic non-methane volatile organic compound (NMVOC) emissions in China during 1990–2017: Drivers, speciation and ozone formation potential. *Atmos. Chem. Phys.* **2019**, *19*, 8897–8913. [CrossRef]
7. Wu, R.; Xie, S. Spatial Distribution of Secondary Organic Aerosol Formation Potential in China Derived from Speciated Anthropogenic Volatile Organic Compound Emissions. *Environ. Sci. Technol.* **2018**, *52*, 8146–8156. [CrossRef] [PubMed]

8. Guenther, A.; Zimmerman, P.; Wildermuth, M. Natural volatile organic compound emission rate estimates for U.S. woodland landscapes. *Atmos. Environ.* **1994**, *28*, 1197–1210. [CrossRef]
9. Wang, F.; Zhang, Z.; Wang, G.; Wang, Z.; Li, M.; Liang, W.; Gao, J.; Wang, W.; Chen, D.; Feng, Y.; et al. Machine learning and theoretical analysis release the non-linear relationship among ozone, secondary organic aerosol and volatile organic compounds. *J. Environ. Sci.* **2022**, *114*, 75–84. [CrossRef]
10. Li, Q.; Su, G.; Li, C.; Liu, P.; Zhao, X.; Zhang, C.; Sun, X.; Mu, Y.; Wu, M.; Wang, Q.; et al. An investigation into the role of VOCs in SOA and ozone production in Beijing, China. *Sci. Total Environ.* **2020**, *720*, 137536. [CrossRef]
11. Tsiligiannis, E.; Hammes, J.; Salvador, C.M.; Mentel, T.F.; Hallquist, M. Effect of NOx on 1,3,5-trimethylbenzene (TMB) oxidation product distribution and particle formation. *Atmos. Chem. Phys.* **2019**, *19*, 15073–15086. [CrossRef]
12. Mao, Y.-H.; Yu, S.; Shang, Y.; Liao, H.; Li, N. Response of Summer Ozone to Precursor Emission Controls in the Yangtze River Delta Region. *Front. Environ. Sci.* **2022**, *10*, 864897. [CrossRef]
13. Zhang, K.; Li, L.; Huang, L.; Wang, Y.; Huo, J.; Duan, Y.; Wang, Y.; Fu, Q. The impact of volatile organic compounds on ozone formation in the suburban area of Shanghai. *Atmos. Environ.* **2020**, *232*, 117511. [CrossRef]
14. Xu, Z.; Huang, X.; Nie, W.; Chi, X.; Xu, Z.; Zheng, L.; Sun, P.; Ding, A. Influence of synoptic condition and holiday effects on VOCs and ozone production in the Yangtze River Delta region, China. *Atmos. Environ.* **2017**, *168*, 112–124. [CrossRef]
15. Batterman, S.A.; Hedin, L.O.; van Breugel, M.; Ransijn, J.; Craven, D.J.; Hall, J.S. Key role of symbiotic dinitrogen fixation in tropical forest secondary succession. *Nature* **2013**, *502*, 224–227. [CrossRef]
16. Jones, M.R.; Pinto, E.; Torres, M.A.; Dörr, F.; Mazur-Marzec, H.; Szubert, K.; Tartaglione, L.; Dell'Aversano, C.; Miles, C.O.; Beach, D.G.; et al. CyanoMetDB, a comprehensive public database of secondary metabolites from cyanobacteria. *Water Res.* **2021**, *196*, 117017. [CrossRef] [PubMed]
17. Jiang, X.; Gao, H.; Zhang, L.; Liang, H.; Zhu, X. Rapid evolution of tolerance to toxic Microcystis in two cladoceran grazers. *Sci. Rep.* **2016**, *6*, 25319. [CrossRef] [PubMed]
18. Rast, A.; Schaffer, M.; Albert, S.; Wan, W.; Pfeffer, S.; Beck, F.; Plitzko, J.M.; Nickelsen, J.; Engel, B.D. Biogenic regions of cyanobacterial thylakoids form contact sites with the plasma membrane. *Nat. Plants* **2019**, *5*, 436–446. [CrossRef] [PubMed]
19. Wu, H.; Wu, X.; Yang, T.; Wang, C.; Tian, C.; Xiao, B.; Lorke, A. Feedback regulation of surface scum formation and persistence by self-shading of Microcystis colonies: Numerical simulations and laboratory experiments. *Water Res.* **2021**, *194*, 116908. [CrossRef]
20. Schindler, D.W.; Hecky, R.E.; Findlay, D.L.; Stainton, M.P.; Parker, B.R.; Paterson, M.J.; Beaty, K.G.; Lyng, M.; Kasian, S.E.M. Eutrophication of lakes cannot be controlled by reducing nitrogen input: Results of a 37-year whole-ecosystem experiment. *Proc. Natl. Acad. Sci. USA* **2008**, *105*, 11254–11258. [CrossRef]
21. Schindler, D.W.; Carpenter, S.R.; Chapra, S.C.; Hecky, R.E.; Orihel, D.M. Reducing Phosphorus to Curb Lake Eutrophication is a Success. *Environ. Sci. Technol.* **2016**, *50*, 8923–8929. [CrossRef] [PubMed]
22. Xu, H.; Qin, B.; Paerl, H.W.; Peng, K.; Zhang, Q.; Zhu, G.; Zhang, Y. Environmental controls of harmful cyanobacterial blooms in Chinese inland waters. *Harmful Algae* **2021**, *110*, 102127. [CrossRef] [PubMed]
23. Wuethrich, B. How Climate Change Alters Rhythms of the Wild. *Science* **2001**, *287*, 793–795. [CrossRef] [PubMed]
24. Walther, G.-R.; Post, E.; Convey, P.; Menzel, A.; Parmesan, C.; Beebee, T.J.C.; Fromentin, J.-M.; Hoegh-Guldberg, O.; Bairlein, F. Ecological responses to recent climate change. *Nature* **2002**, *416*, 389–395. [CrossRef] [PubMed]
25. Hou, X.; Feng, L.; Dai, Y.; Hu, C.; Gibson, L.; Tang, J.; Lee, Z.; Wang, Y.; Cai, X.; Liu, J.; et al. Global mapping reveals increase in lacustrine algal blooms over the past decade. *Nat. Geosci.* **2022**, *15*, 130–134. [CrossRef]
26. Fang, C.; Song, K.; Paerl, H.W.; Jacinthe, P.-A.; Wen, Z.; Liu, G.; Tao, H.; Xu, X.; Kutser, T.; Wang, Z.; et al. Global divergent trends of algal blooms detected by satellite during 1982–2018. *Glob. Chang. Biol.* **2022**, *28*, 2327–2340. [CrossRef]
27. Trolle, D.; Elliott, J.A.; Mooij, W.M.; Janse, J.H.; Bolding, K.; Hamilton, D.P.; Jeppesen, E. Advancing projections of phytoplankton responses to climate change through ensemble modelling. *Environ. Model. Softw.* **2014**, *61*, 371–379. [CrossRef]
28. Woolway, R.I.; Kraemer, B.M.; Lenters, J.D.; Merchant, C.J.; O'Reilly, C.M.; Sharma, S. Global lake responses to climate change. *Nat. Rev. Earth Environ.* **2020**, *1*, 388–403. [CrossRef]
29. Qin, B.Q.; Zhou, J.; Elser, J.J.; Gardner, W.S.; Deng, J.M.; Brookes, J.D. Water Depth Underpins the Relative Roles and Fates of Nitrogen and Phosphorus in Lakes. *Environ. Sci. Technol.* **2020**, *54*, 3191–3198. [CrossRef]
30. Bouvy, M.; Nascimento, S.M.; Molica, R.J.R.; Ferreira, A.; Huszar, V.; Azevedo, S.M.F.O. Limnological features in Tapacurá reservoir (northeast Brazil) during a severe drought. *Hydrobiologia* **2003**, *493*, 115–130. [CrossRef]
31. Zhao-tang, S.; Jian, R.E.N.; Ming-rong, Q.I.N.; Ying, X.I.A.; Lang, H.E.; Yu-wen, C. Relationships between climatic change and cyanobacterial bloom in Taihu Lake. *Chin. J. Ecol.* **2010**, *29*, 55–61.
32. Wang, M.; Zhan, Y.; Chen, C.; Chen, M.; Zhu, J.; Jiang, X.; Yang, Y.; Lv, X.; Yin, P.; Zhang, W.; et al. Amplified cyanobacterial bloom is derived by polyphosphate accumulation triggered by ultraviolet light. *Water Res.* **2022**, *222*, 118837. [CrossRef] [PubMed]
33. Carrick, H.J.; Aldridge, F.J.; Schelske, C.L. Wind Influences phytoplankton biomass and composition in a shallow, productive lake. *Limnol. Oceanogr.* **1993**, *38*, 1179–1192. [CrossRef]

34. Wu, T.; Qin, B.; Brookes, J.D.; Shi, K.; Zhu, G.; Zhu, M.; Yan, W.; Wang, Z. The influence of changes in wind patterns on the areal extension of surface cyanobacterial blooms in a large shallow lake in China. *Sci. Total Environ.* **2015**, *518–519*, 24–30. [CrossRef] [PubMed]
35. Liu, J.; Zhang, Y.; Qian, X.; Qian, Y. Review of cyanobacteria remote sensing in Taihu Lake. *Environ. Pollut. Control.* **2009**, *31*, 79–83.
36. Shi, K.; Zhang, Y.L.; Qin, B.Q.; Zhou, B.T. Remote sensing of cyanobacterial blooms in inland waters: Present knowledge and future challenges. *Sci. Bull.* **2019**, *64*, 1540–1556. [CrossRef] [PubMed]
37. Wang, M.; Zheng, W.; Liu, C. Application of Himawari-8 data with high-frequency observation for Cyanobacteria bloom dynamically monitoring in Lake Taihu. *J. Lake Sci.* **2017**, *29*, 1043–1053.
38. Feng, L. Key issues in detecting lacustrine cyanobacterial bloom using satellite remote sensing. *J. Lake Sci.* **2021**, *33*, 647–652.
39. Ho, J.C.; Michalak, A.M.; Pahlevan, N. Widespread global increase in intense lake phytoplankton blooms since the 1980s. *Nature* **2019**, *574*, 667–670. [CrossRef]
40. Dörnhöfer, K.; Oppelt, N. Remote sensing for lake research and monitoring—Recent advances. *Ecol. Indic.* **2016**, *64*, 105–122. [CrossRef]
41. Alharbi, B. Remote sensing techniques for monitoring algal blooms in the area between Jeddah and Rabigh on the Red Sea Coast. *Remote Sens. Appl.-Soc. Environ.* **2023**, *30*, 100935. [CrossRef]
42. Kefauver, S.C.; Filella, I.; Peñuelas, J. Remote sensing of atmospheric biogenic volatile organic compounds (BVOCs) via satellite-based formaldehyde vertical column assessments. *Int. J. Remote Sens.* **2014**, *35*, 7519–7542. [CrossRef]
43. Xing, C.Z.; Liu, C.; Hu, Q.H.; Fu, Q.Y.; Lin, H.; Wang, S.T.; Su, W.J.; Wang, W.W.; Javed, Z.; Liu, J.G. Identifying the wintertime sources of volatile organic compounds (VOCs) from MAX-DOAS measured formaldehyde and glyoxal in Chongqing, southwest China. *Sci. Total Environ.* **2020**, *715*, 136258. [CrossRef] [PubMed]
44. Vrekoussis, M.; Wittrock, F.; Richter, A.; Burrows, J.P. GOME-2 observations of oxygenated VOCs: What can we learn from the ratio glyoxal to formaldehyde on a global scale? *Atmos. Chem. Phys.* **2010**, *10*, 10145–10160. [CrossRef]
45. Su, W.J.; Liu, C.; Chan, K.L.; Hu, Q.H.; Liu, H.R.; Ji, X.G.; Zhu, Y.Z.; Liu, T.; Zhang, C.X.; Chen, Y.J.; et al. An improved TROPOMI tropospheric HCHO retrieval over China. *Atmos. Meas. Tech.* **2020**, *13*, 6271–6292. [CrossRef]
46. Paerl, H.W.; Otten, T.G. Harmful Cyanobacterial Blooms: Causes, Consequences, and Controls. *Microb. Ecol.* **2013**, *65*, 995–1010. [CrossRef]
47. Xiao, Q.T.; Zhang, M.; Hu, Z.H.; Gao, Y.Q.; Hu, C.; Liu, C.; Liu, S.D.; Zhang, Z.; Zhao, J.Y.; Xiao, W.; et al. Spatial variations of methane emission in a large shallow eutrophic lake in subtropical climate. *J. Geophys. Res.-Biogeosci.* **2017**, *122*, 1597–1614. [CrossRef]
48. Zhang, X.Y.; Friedl, M.A.; Schaaf, C.B.; Strahler, A.H.; Hodges, J.C.F.; Gao, F.; Reed, B.C.; Huete, A. Monitoring vegetation phenology using *Modis*. *Remote Sens. Environ.* **2003**, *84*, 471–475. [CrossRef]
49. Jingping, X.U.; Ba, Z.; Fang, L.I.; Kaishan, S.; Zongming, W. Detecting modes of cyanobacteria bloom using MODIS data in Lake Taihu. *Sci. Limnol. Sin.* **2008**, *20*, 191–195. [CrossRef]
50. Zhang, H.; Gu, K.; Zhang, S. Extracting temporal and spatial distribution features of Lake Taihu from MODIS-EVI data by empirical orthogonal function analysis. *Chin. J. Ecol.* **2018**, *37*, 3802–3808.
51. Xiao, Y.; Zhang, J.; Cui, T.; Gong, J.; Liu, R.; Chen, X.; Liang, X. Remote sensing estimation of the biomass of floating *Ulva prolifera* and analysis of the main factors driving the interannual variability of the biomass in the Yellow Sea. *Mar. Pollut. Bull.* **2019**, *140*, 330–340. [CrossRef] [PubMed]
52. Peng, S.; Ding, Y.; Liu, W.; Li, Z. 1 km monthly temperature and precipitation dataset for China from 1901 to 2017. *Earth Syst. Sci. Data* **2019**, *11*, 1931–1946. [CrossRef]
53. Yu, Y.-j.; Li, C.-y.; Shen, W.; Wang, Z.; Xu, P.-q.; Yu, H.-x. Volatile compounds released by microalgae-water phase from Taihu Lake in China. *Harmful Algae* **2019**, *84*, 56–63. [CrossRef] [PubMed]
54. Liu, M.; Wu, T.; Zhao, X.; Zan, F.; Yang, G.; Miao, Y. Cyanobacteria blooms potentially enhance volatile organic compound (VOC) emissions from a eutrophic lake: Field and experimental evidence. *Environ. Res.* **2021**, *202*, 111664. [CrossRef] [PubMed]
55. Ke, G.L.; Meng, Q.; Finley, T.; Wang, T.F.; Chen, W.; Ma, W.D.; Ye, Q.W.; Liu, T.Y. LightGBM: A Highly Efficient Gradient Boosting Decision Tree. In Proceedings of the Advances in Neural Information Processing Systems 30 (NIPS 2017), Long Beach, CA, USA, 4–9 December 2017.
56. Bentéjac, C.; Csörgo, A.; Martínez-Muñoz, G. A comparative analysis of gradient boosting algorithms. *Artif. Intell. Rev.* **2021**, *54*, 1937–1967. [CrossRef]
57. Dai, Y.; Yang, S.; Zhao, D.; Hu, C.; Xu, W.; Anderson, D.M.; Li, Y.; Song, X.-P.; Boyce, D.G.; Gibson, L.; et al. Coastal phytoplankton blooms expand and intensify in the 21st century. *Nature* **2023**, *615*, 280–284. [CrossRef] [PubMed]
58. Zhang, M.M.; Shao, M.; Chen, P.; Gu, C.; Wang, Q.G. Comparative study of anthropogenic and biogenic VOCs emission characteristics and their impact on O_3 and SOA formation potential in the Yangtze River Delta region. *China Environ. Sci.* **2023**, 1–12. [CrossRef]
59. An, J.; Huang, Y.; Huang, C.; Wang, X.; Yan, R.; Wang, Q.; Wang, H.; Jing, S.; Zhang, Y.; Liu, Y.; et al. Emission inventory of air pollutants and chemical speciation for specific anthropogenic sources based on local measurements in the Yangtze River Delta region. *Atmos. Chem. Phys.* **2021**, *21*, 2003–2025. [CrossRef]

60. Zhou, Y.; Zhao, Y.; Mao, P.; Zhang, Q.; Zhang, J.; Qiu, L.; Yang, Y. Development of a high-resolution emission inventory and its evaluation and application through air quality modeling for Jiangsu Province, China. *Atmos. Chem. Phys.* **2017**, *17*, 211–233. [CrossRef]
61. Cui, L.; Xiao, Y.; Hu, W.; Song, L.; Wang, Y.; Zhang, C.; Fu, P.; Zhu, J. Enhanced dataset of global marine isoprene emissions from biogenic and photochemical processes for the period 2001–2020. *Earth Syst. Sci. Data* **2023**, *15*, 5403–5425. [CrossRef]